Chapter III. Plasma-material interactions in magnetic fusion devices

The choice of material for a fusion reactor is a complex problem, which concerns both the structural and PFCs materials facing different requirements such as material resilience to high heat fluxes and neutron fluence (e.g. see [1] and the references therein). Here we only consider the PFC materials. The plasma-material interaction for fusion relevant conditions is a relatively young area of research where our understanding of the physics involved is still incomplete. Therefore, in this chapter, we will focus on the issues that, we believe, are the most important for the description of edge plasma processes on the one hand and, on the other hand, the physics of which is reasonably well understood and verified. In addition, we will also discuss some gaps in our understanding/description of plasma material interactions in magnetic fusion devices.

Usually, it is assumed that the major issues of plasma interaction with the materials of the PFCs are related to the PFCs erosion (determining the PFCs lifetime) and tritium retention. For example, carbon had been dismissed as the PFC material for ITER based on the assessment of tritium retention [2], which was later, to some extent, confirmed experimentally [3]. However, there is still a need for both better assessment of tritium retention in the materials potentially suitable for the PFCs and understanding of other phenomena related to plasma-material interaction in future reactors.

The processes taking place at the surface and within some depth beneath the surface of the PFCs in fusion devices are very complex and diverse. They determine a wide spectrum of different phenomena including erosion of the PFC material, plasma contamination with impurity, plasma recycling and tritium retention, dust formation, modification of the surface morphology and the physical properties of the under-surface material, etc. Many of these processes depend not only on the particular material but also on the temperature, the constituency of plasma species and their energies. One of the complications in the study of the physics of plasma-material interactions for fusion-relevant conditions is a strong modification of the original material during its exposure to plasma in the fusion devices (see Fig. III.1). This can be related to many factors including a strong saturation of the near-surface material layer with hydrogen/helium caused by plasma bombardment, formation of co-deposited layers (due to transport of the eroded material) which have physical properties different from the original ones (e.g. amorphous rather than crystal structure), melting with further re-crystallization, resulting in the change of the grain size, etc.

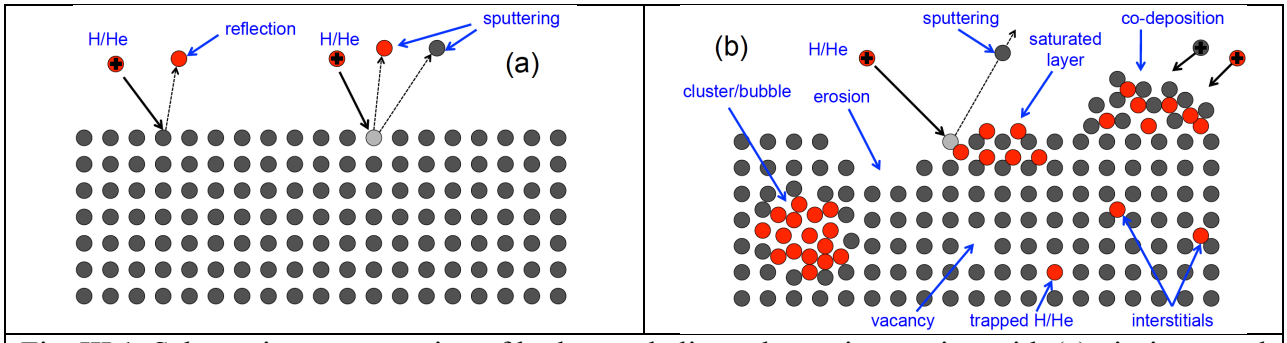

Fig. III.1. Schematic representation of hydrogen-helium plasma interaction with (a) virgin crystal structure of the PFM and (b) modified material structure after plasma exposure.

Different experimental and theoretical techniques are used for the study of particular features of the phenomena related to the PFM in a fusion plasma environment. For example, on the experimental side, the optical and different kind of electron microscope (e.g. tunneling, TEM, and secondary emission, SEM, electron microscopes) images of material surfaces exposed to the plasma are often used to monitor the surface morphology modification (e.g. see Fig. III.2), whereas the temperature desorption spectra (TDS) and nuclear reaction analysis (NRA) along with other methods are used both to infer the concentrations of hydrogen and helium trapped in the plasma-facing materials and to shed some light on the possible trapping mechanisms (e.g. see Fig. III.3). We notice that most of the experimental data on plasma-material interactions come from specially designed experiments performed on relatively small-scale linear devices with well-characterized plasma parameters. However, tokamak experiments provide the data on plasma-material interactions for the "real" tokamak plasma environment, which is often characterized by violent anomalous transport phenomena in multi-species plasma and a long-range migration of the eroded material.

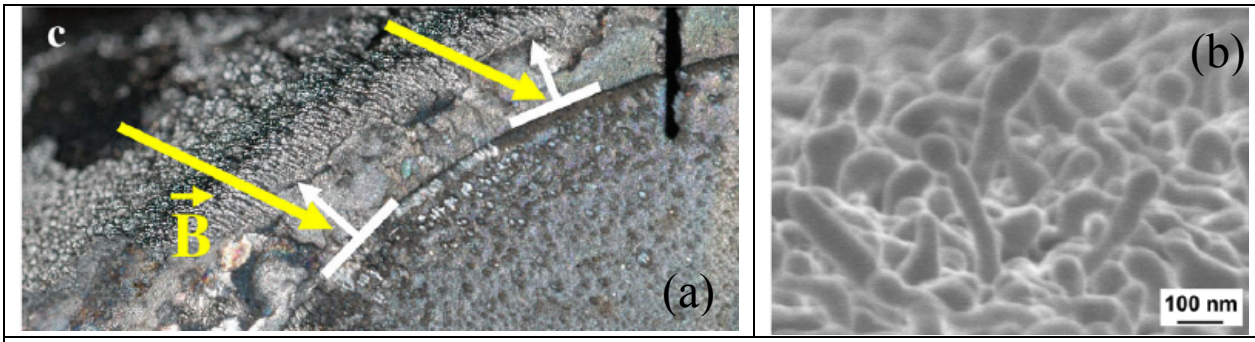

Fig. III.2. (a) optical image of carbon co-deposits on the leading edge of Tore Supra neutralizer (Reproduced with permission from [4], © Elsevier 2009) and (b) SEM picture of "nano-fuzz" rods growing on tungsten surface under helium irradiation (Reproduced with permission from [5], © IAEA 2009).

On the theoretical side, the approaches to study of the PFM-related physics range from the first-principle codes utilizing the density functional theory (DFT) [7] (e.g. QUANTUM-ESPRESSO [8], VASP [9]) to the simulations of particular, relatively small-scale features with different versions of Molecular Dynamic (MD) and Monte Carlo (MC) codes (e.g. LAMMPS [10], TRYDIN [11]), and to the study of macroscopic phenomena with the codes based on the continuum reaction-diffusion approximation (e.g. TMAP [12], [13], FACE [14]) and semi-analytic models. Whereas the DFT-based simulations are capable of treating only a few tens of atoms and are usually used to determine the binding energies of the hydrogen and helium atoms in different lattice defects in fusion-relevant materials and to infer the inter-particle interaction potentials, the MD simulations employing complex multi-particle interaction potentials can describe phenomena associated with the dynamics of millions of particles (e.g. the formation of the helium nano-bubbles in tungsten, see Fig. III.4), and the reaction-diffusion-based codes are used to simulate such macroscopic features as hydrogen and helium transport and trapping in the fusion-related materials and to interpret the TDS data.

However, in practice application of even MD simulations to the study of many important practical problems (e.g. nucleation and growth of the fuzz shown in Fig. III.2b) is beyond both the present and near-future computer capabilities. In addition, interatomic potentials used in the

MD simulations do not always result in the physically meaningful outcomes (e.g. see [16]). On the other hand, the reaction-diffusion-based codes, which can be used for the long-time, large-scale simulations, rely on the transport properties of the species of interest (e.g. hydrogen and helium) and the rate constants of different "reactions".

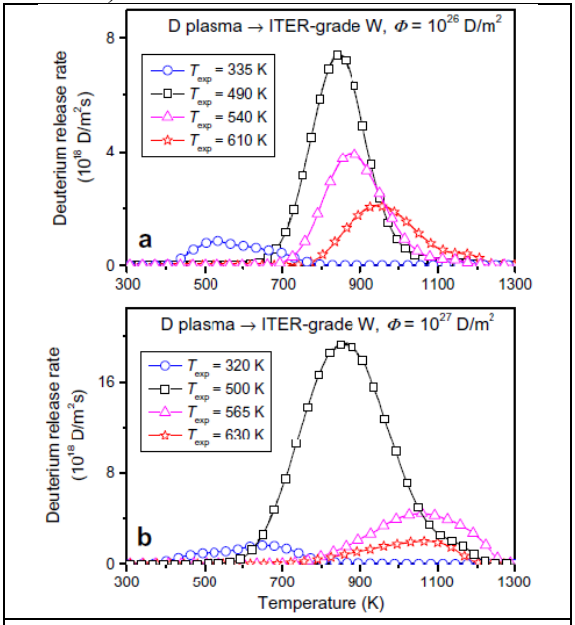

Fig. III.3. TDS data showing D release from ITER-grade tungsten irradiated by 38 eV deuterium ions with the flux 10^{22} m^2/s and fluences 10^{26} (a) and 10^{27} D/m^2 (b) at various temperatures. Reproduced with permission from [6], © IOP Publishing 2014.

These hydrogen and helium transport models, as well as the rate constants, which are either taken from some *ad hoc* assumptions or deduced from the MD simulations, in most cases, do not allow for the effects of lattice stress, which can play an important role in many different phenomena.

As a result, understanding of the physics involved in the fusion plasma-material-related phenomena in many cases is still rather poor. Therefore, in this chapter, we will consider only the most generic features of the plasma interactions with the PFC materials in a magnetic fusion environment and give short reviews of some interesting phenomena, even though their physics might be not entirely clear yet. Further details of the current research activities, considering both solids (beryllium and tungsten) and liquids (lithium, tin) as potential materials for the PFCs, can be found in relevant review papers (e.g. see [17] [18], [19], [20], [6], [21], [22] [23], [24], [25]) and original journal publications.

III.1 Reflection of plasma particles impinging on material surfaces and sputtering of plasma-facing materials

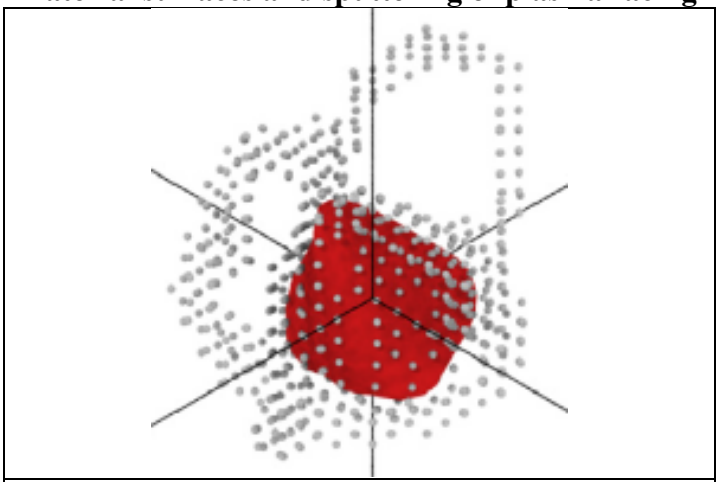

Fig. III.4. MD simulations of growing helium nano-bubble in tungsten emitting dislocation loops. Helium atoms are in red and displaced tungsten atoms are in grey colors. Reproduced with permission from [15], © Elsevier 2015.

Both reflection and absorption of plasma particles (in particular, hydrogen and helium) impinging on material surfaces result in the edge plasma energy and particle sinks and, therefore, are crucially important for the plasma recycling process. In addition, the accompanying processes of sputtering of the plasma-facing materials are essential for plasma contamination with impurity and erosion of the PFCs.

We start with the particle and energy reflection coefficients. Whereas the particle reflection coefficient, R_N, is just the probability of particle impinging on the target surface to be reflected back, the energy reflection coefficient,

R_E, needs some clarification. The reflected particles usually have a broad energy distribution function having an average value $\langle E_R \rangle$. For example, for the case where a light projectile strikes a target of heavy elements (e.g. tungsten), some reflected particles have the energy close to the initial projectile energy, E_p. Therefore, for accurate treatment of the energy of the reflected particles with MC neutral codes used in the edge plasma studies, one should consider the whole energy spectrum of the reflected particles. However, for some crude estimates one can use the average energy $\langle E_R \rangle$, which can be expressed in terms of R_N, R_E, and E_p as follows:

$$\langle E_R \rangle = E_p R_E / R_N . \qquad \text{(III.1)}$$

The energy dependence of the particle and energy reflection coefficients of both hydrogen and helium within the energy range of interest (from ~10 eV to ~1 keV) for the case of normal incidence onto the target can be described by the following expression [26]

$$R_{N/E} = \frac{A_1^{N/E} \ell n\left(A_2^{N/E} \varepsilon_p + e\right)}{1 + A_3^{N/E} (\varepsilon_p)^{A_4^{N/E}} + A_5^{N/E} (\varepsilon_p)^{A_6^{N/E}}}, \qquad \text{(III.2)}$$

where ε_p is the Thomas-Fermi reduced energy of the projectile

$$\varepsilon_p = 3.255 \times 10^{-2} \frac{M_t / M_p}{1 + M_t / M_p} \frac{E_p[\text{eV}]}{Z_p Z_t \left(Z_p^{2/3} + Z_t^{2/3}\right)^{1/2}}, \qquad \text{(III.3)}$$

M_p (M_t) and Z_p (Z_t) are the mass and charge of the projectile (target) nuclei and $E_p[\text{eV}]$ is the projectile energy in eV. The coefficients $A_{(...)}^{N/E}$, taken from [26], can be found in Table III.1

However, the expression (III.2) fails to reproduce the reflection coefficients at low E_p (below ~ a few eV). For example, from Eq. (III.2) and the data from Table III.1, it follows that the reflection coefficient of a low energy ^{4}He from tungsten is ~0.8. However, more close consideration shows that in order to penetrate into the tungsten lattice and have a chance to be trapped there, the helium particle has to overcome a potential barrier ~ 6 eV [27]. Therefore, the helium reflection coefficient from pure tungsten target should be equal to unity for the helium kinetic energy below this potential barrier. The situation with hydrogen impinging on the tungsten target is more complex since hydrogen can be chemically adsorbed on the tungsten surface (e.g. see [28] and the references therein).

Next, we consider the so-called physical sputtering of the targets. Physical sputtering assumes no formation of chemical bonds between the projectile and the target particles. The probability of the projectile to sputter a target particle (sputtering yield) depends on both the projectile energy E_p and the incidence angle. For the normal incidence, the yield of physical sputtering $Y_{ph}(E_p)$ is given by the following expression [19]

$$Y_{ph}(E_p) = A_1^{sp} f(\varepsilon_p) \frac{(E_p / E_{th} - 1)^{A_2^{sp}}}{A_3^{sp} + (E_p / E_{th} - 1)^{A_2^{sp}}}, \qquad \text{(III.4)}$$

where E_{th} is the sputtering threshold energy, $A_{(...)}^{sp}$ are the fitting parameters and the function $f(\varepsilon_p)$ is given by the following formula

$$f(\varepsilon_p) = \frac{0.5\ell n(1 + 1.2288\varepsilon_p)}{\varepsilon_p + 0.1728\sqrt{\varepsilon_p} + 0.008(\varepsilon_p)^{0.1504}}. \qquad \text{(III.5)}$$

Table III.1. Fitting parameters $A_{(...)}^{N/E}$ for both the particle and energy reflection coefficients. Reproduced with permission from [19], © Springer 2007.

	$A_1^{N/E}$	$A_2^{N/E}$	$A_3^{N/E}$	$A_4^{N/E}$	$A_5^{N/E}$	$A_6^{N/E}$
$R_N\ (M_t / M_p > 20)$	0.8250	21.41	8.606	0.6425	1.907	1.927
$R_E\ (M_t / M_p > 20)$	0.6831	27.16	15.66	0.6598	7.967	1.822
$R_N\ (M_t / M_p = 3)$	0.3680	2.985	7.122	0.5802	4.211	1.597
$R_E\ (M_t / M_p = 3)$	0.2058	3.848	19.07	0.4872	15.13	1.638

We notice that the surface binding energy, E_s, of Be, W, and Li has values of 3.38, 8.68 and 1.67 eV respectively, which are, as follows from Table III.2, significantly lower than E_{th}, in particular, for the case of a large mass ratio of the target to projectile atoms. This is not surprising, since according to the binary collision approximation, the maximum relative energy transfer between the two particles is $4M_pM_t / (M_p + M_t)^2$, which is small for $M_p << M_t$ (e.g. for the collisions of hydrogenic species with tungsten atoms).

Both the reflection coefficients and the sputtering yields depend also on the projectile incidence angle, ϑ_p. Whereas the particle reflection coefficient increases with increasing ϑ_p, the yield of physical sputtering, having a minimum at the normal incidence, initially increases also with increasing ϑ_p, reaches a maximum at some angle $(\vartheta_p)_{max} < \pi / 2$ and then drops to a virtually zero value. Although the particular angular dependence of $Y_{ph}(E_p, \vartheta_p)$ is significant, rather complex and sensitive to E_p (e.g. see Fig. III.5 and Ref. [19] for further details), in practice, for the edge plasma conditions where the distribution function of the particles impinging on the target has a broad angular and energy spread, this effect does not result in any specific feature of the average sputtering yield. In addition, the surface roughness also smears out the angular dependence of sputtering.

Although physical sputtering should not depend on the target temperature, the experimental data undoubtedly show that starting with some elevated temperature, the yield of

physical sputtering of different solid (e.g. Ag, Bi, Cu, Ge, Zn, [29] and the references therein, W [30], C [31], Be [32]) and liquid (e.g. Li [33], [34], Ga [35]) materials strongly increases with increasing target temperature. Theoretical explanations of this effect are ranging from different variations of an old idea of formation of a "hot spot" around the striking point of the projectile [36] to the creation of the Frenkel pairs (in a carbon target) [37] with further diffusion of the interstitial carbon atoms to the surface and their subsequent evaporation. However, for different reasons, these models are unable to fit the available experimental data. It seems that at this moment, the model based on the idea of "adatoms" (the target atoms that are "splashed" to the target surface in the course of the projectile-target interactions) [32] shows the best agreement with the experimental data for both the solid and liquid materials (see Fig. III.6).

Table III.2. Threshold energy E_{th} and the fitting parameters $A^{sp}_{(...)}$ for the physical sputtering of Be, W and Li by H, D, T, ^{4}He, self-sputtering, N, and Ne. Reproduced with permission from [19], © Springer 2007.

	H	D	T	^{4}He	Self	N	Ne
Be							
E_{th} (eV)	14.3	9.5	9.4	12.3	17	16.5	22.8
A^{sp}_1	0.0564	0.1044	0.1379	0.3193	0.8241	0.9334	1.8309
A^{sp}_2	1.5147	1.9906	1.5660	1.6989	1.3437	2.5368	1.9400
A^{sp}_3	0.8007	1.7575	2.0794	1.7545	2.0334	5.2833	2.5474
W							
E_{th} (eV)	457	228.8	153.9	120.6	25	45.5	38.6
A^{sp}_1	0.0075	0.0183	0.0419	0.1151	18.6006	1.4389	2.5520
A^{sp}_2	1.2046	1.4410	1.5802	1.7121	3.1273	2.0225	1.9534
A^{sp}_3	1.0087	0.3583	0.2870	0.1692	2.2697	0.0921	0.0828
Li							
E_{th} (eV)	5.56	4.6	4.86	6.5	5.5		
A^{sp}_1	0.0833	0.1321	0.1629	0.3617	0.5159	-	-
A^{sp}_2	1.4705	1.2091	0.9741	1.2501	1.7546		
A^{sp}_3	0.9540	1.4358	1.8839	1.9370	8.2237		

Whereas the energy distribution of the atoms sputtered via the "standard" physical sputtering process follow the Thompson distribution [38]

$$f_{Th}(E) \propto \frac{E}{(E+E_s)^3}, \qquad \text{(III.6)}$$

the atoms sputtered due to the temperature-induced effects have the energy dependence determined by the target temperature (e.g. see [39]).

The sputtering processes discussed so far do not involve the possible formation of chemical bonds between the projectile and the target atoms. However, "chemical" effects, resulting in the so-called chemical sputtering, could be for some cases the dominant sputtering mechanism. In particular, irradiation of a carbon target with hydrogen, even at low energies, results in the formation of volatile hydrocarbon molecules, which could dominate the carbon erosion (e.g. see [19] and the references therein). However, we notice that the formation of the chemical bonds between the projectile and the target atoms does not necessarily result in chemical sputtering. For example, in Ref. [40] it was found that beryllium irradiation with hydrogen results in the formation of beryllium hydride, but, unlike hydrocarbons, it is not volatile and, therefore, does not contribute to the chemical erosion mechanism.

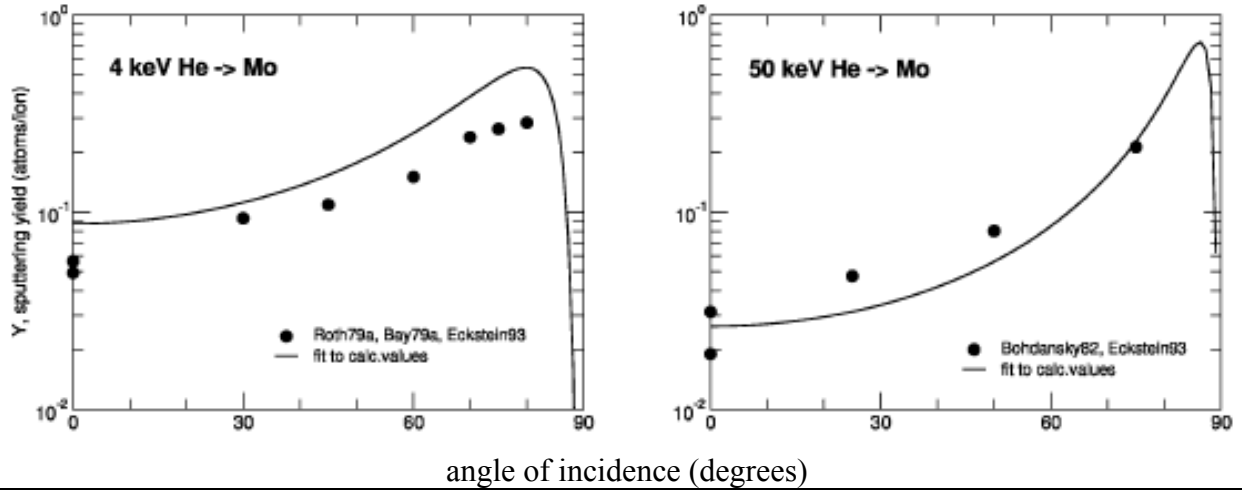

Fig. III.5. Sputtering yields of molybdenum by 4 keV (left) and 50 keV (right) helium ions as a function of the incidence angle. The dots are the experimental data and the solid lines are the fits. Reproduced with permission from [19], © Springer 2007.

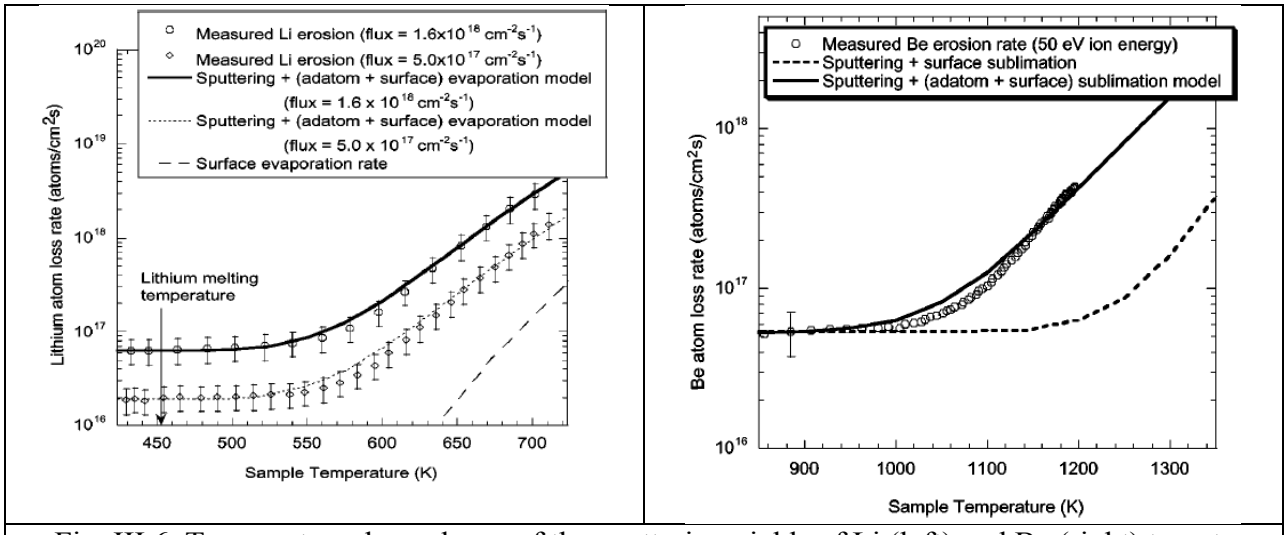

Fig. III.6. Temperature dependence of the sputtering yields of Li (left) and Be (right) targets from both experimental data and theoretical model based on the "adatom" concept. Reproduced with permission from [32], © AIP Publishing 2004.

We also note that both the reflection coefficients and the sputtering yields are sensitive to the constituency of the very first atomic layers of the target, which can be altered by mixing/implantation of different target materials (e.g. Be and W) or by the saturation of these layers with hydrogen or helium.

III.2 Basic features of hydrogen/helium transport in plasma-facing materials

Once the hydrogen and/or helium atoms penetrate into the PFC material lattice, they become the subjects of complex multi-body interactions with the lattice atoms. For illustration purposes, these interactions are often portrayed as a motion of the hydrogen or helium atoms through effective potential structures (see Fig. III.7). Such a motion of the hydrogen or helium atoms is assumed to be "strongly dumped", which implies that the total particle energy (kinetic plus potential) is not conserved because of the multi-body nature of the particle interactions. The spacing between the local, relatively small (~0.4 eV) minima of the potential energy is determined by the lattice arrangement (recall that it has a 3D structure). Due to thermal effects, the particles can move from one minimum to another one in a random way, so that in the simplest case, dynamics of the hydrogen and helium atoms can be described by a diffusion process with the diffusion coefficient $D \propto \exp(-E_{dif}/T)$, where E_{dif} is the "depth" of the local potential well which depends on both the material and the diffusing particle (e.g. for tungsten we have $E_{dif}^{H} \approx 0.25\,\text{eV}$ and $E_{dif}^{He} \approx 0.15\,\text{eV}$). However, in practice, the lattice arrangement is not perfect and has some defects (e.g. vacancies, dislocations). In most cases, the effective potential well associated with these lattice defects, E_{tr}, for both the hydrogen and helium atoms is significantly deeper than E_{dif}. As a result, the atoms become virtually "trapped" in these deep potential wells where E_{tr} is often in the range of 1÷2 eV and even higher (e.g. see [41], [42], [43] [44] and the references therein). In practice, the release of particles from such traps is only possible either for relatively high target temperatures or over a long time.

To describe hydrogen and/or helium transport in the material lattice on large spatiotemporal scales, the reaction-diffusion (RD) model is often used. The RD model deals with free (mobile interstitial) and trapped (usually immobile) hydrogen and/or helium atoms. The free atoms can be trapped in and de-trapped from the trapping sites. For the simplest case where we assume that there is only one kind of traps having the density, N_{tr}, which can trap only one atom, the RD equations describing the free and immobile trapped atom densities, n_f, and, n_{tr}, can be written as follows

$$\frac{\partial n_f}{\partial t} = \nabla\cdot\left(D\nabla n_f\right) - K_{tr} n_f \left(N_{tr} - n_{tr}\right) + \nu_{dtr} n_{tr}, \qquad \text{(III.7)}$$

$$\frac{\partial n_{tr}}{\partial t} = K_{tr} n_f \left(N_{tr} - n_{tr}\right) - \nu_{dtr} n_{tr}, \qquad \text{(III.8)}$$

where K_{tr} is the trapping rate constant, $\nu_{dtr} = \nu_0 \exp(-E_{tr}/T)$ is the de-trapping frequency and ν_0 is the bounce frequency of the atom in the trapping potential well. The rate constant K_{tr} is often described in a diffusive approximation, assuming that the free atom becomes trapped when it approaches the trapping site at a distance R_{tr}. Then, considering the diffusion of the free atom

to the trapping site in the dilute approximation (the averaged distance between the trapping sites is larger than R_{tr}), we find $K_{tr} = 4\pi D R_{tr}$.

Although the equations III.7 and III.8 are rather simple, the RD models used in practice quickly become very complex when other effects such as: large amount of the trapping sites with different trapping energies [45], [46]; trapping of few atoms at one trapping site [47]; stress-induced advection of the free atoms [48], [15]; nonlinear generation of new trapping sites and modification of the existing ones [49], [50], [51]; etc. are added.

The boundary conditions, which are needed to close the second-order differential equation (III.7) used for hydrogen and helium transport studies, can be different, which is related to the different structure of the effective hydrogen and helium potentials at the surface as shown in Fig. III.7. Since the free helium atoms are not bound to the surface, one can take zero density of the free helium atoms at the "surface" as the boundary condition for Eq. (III.7). The situation with hydrogen, which can be bounded to the surface, is more complex and depends on the target material. For example, for the case of tungsten, hydrogen is desorbed from the surface as a molecule. As a result, the corresponding boundary conditions should involve some surface recombination rate coefficient, K_{rec}^{surf}, describing the conversion of atomic to molecular hydrogen. However, the available experimental data on K_{rec}^{surf} are very unreliable and differ by orders of magnitude (e.g. see [42] and the references therein). Therefore, it is often assumed (e.g. for the interpretation of the TDS data) that hydrogen transport through the target lattice is limited by volumetric diffusion and trapping/de-trapping processes so that it is possible to assume that the free hydrogen density at the "surface" is zero. Nonetheless, it is plausible that the presence of hydrogen at the surface along with a rather high hydrogen surface potential barrier E_b can significantly alter the penetration and accumulation of the low energy hydrogen species in the target (e.g. [52]). Therefore, the issue of hydrogen absorption at the surface requires further thorough investigation.

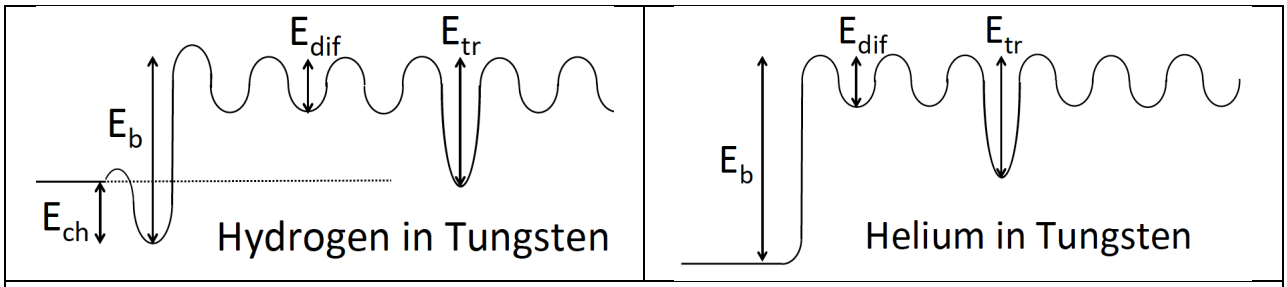

Fig. III.7. Effective hydrogen (left) and helium (right) potential structures illustrating hydrogen and helium transport in tungsten, where E_{dif} is the diffusion activation energy ($E_{dif}^{H} \approx 0.25\,eV$, $E_{dif}^{He} \approx 0.15\,eV$), E_{tr} is the "trapping" energy, E_b is the surface energy barrier ($E_b^{H} \sim 2.5\,eV$, $E_b^{He} \approx 6\,eV$), and E_{ch} is the chemisorption potential well ($E_{ch}^{H} \lesssim 1\,eV$).

Although the RD equations look similar and independent of both the target material and the species transported through its lattice, in practice the mechanisms of the formation of traps and, therefore, the overall dynamics of transport and the characteristic processes associated with it are sensitive to both the target material and the species transported.

Therefore, to be more specific in what follows, we consider the main features of hydrogen and helium behavior in tungsten, which is chosen as the material for the divertor targets in ITER and, therefore, has been studied very extensively in last decade. In addition, tungsten, being irradiated by hydrogen and helium, exhibits interesting physical phenomena, somewhat similar to those observed in other metals (e.g. molybdenum, tantalum, etc. [24]).

Numerous DFT and MD simulations show a very different character of the interactions of few hydrogen and helium atoms with tungsten (e.g. see [24] and the references therein). Unlike hydrogen, the interstitial helium atoms in the tungsten lattice exhibit a strong trend to clustering (formation of binaries, triplets, etc.) even in the absence of lattice defects. For example, in Fig. III.8 one can see an increase of the helium binding energy to the interstitial cluster containing N helium atoms with increasing N, whereas the binding energy for a hydrogen atom to a vacancy decreases with the increasing number of hydrogen atoms.

The formation of the interstitial helium cluster imposes large localized stress on the lattice, which finally results in the creation of the Frenkel pair. This reduces the stress but produces a vacancy, which "frees" the space and promotes absorption of more helium atoms into the cluster. Further amassment of the cluster with "kicking off" the tungsten atoms from the lattice, which is called "trap mutation" (e.g. see [55], [56], [57], [58]), is often considered to be the mechanism of helium nano-bubble growth in many metals (e.g. see [24] and the references therein).

Since, unlike helium, the interstitial hydrogen clusters do not exhibit self-trapping effects, it is widely believed that the origin of hydrogen trapping (which could finally result in the formation of hydrogen nano-bubbles [59] or relatively large blisters [6]) is associated with lattice defects.

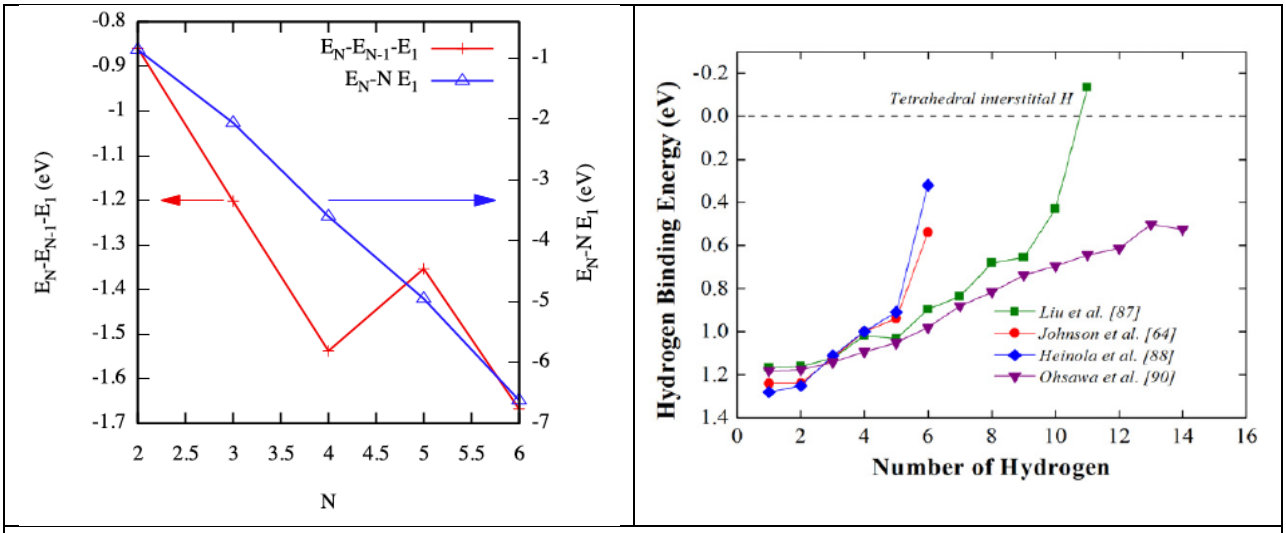

Fig. III.8. On the left, the He binding energy in an interstitial He cluster as a function of N (red curve), reproduced with permission from [53], © American Physical Society 2014; On the right, the H binding energy with a mono-vacancy as a function of the number of hydrogen atoms. Reproduced with permission from [54], © IAEA 2014.

The experimental results demonstrate also very different penetration of helium and hydrogen into tungsten. For example, in Fig. (III.9) one can see that helium nano-bubbles are localized within ~ 30 nm beneath the surface. It was also shown that visible modification of the tungsten target surface morphology induced by helium irradiation starts at the same helium

fluence $\Phi_{layer} \sim 2.5\times10^{24}\,m^{-2}$ even though the flux of helium ions impinging onto the surface in these experiments differs by few orders of magnitude [62]. It implies that the buildup of such a helium-reach sub-layer is not sensitive to the helium flux. From Fig. III.9 one can see that, contrary to helium, hydrogen penetrates into the tungsten sample up to ~10 microns, even though the implantation range of the low energy hydrogen ions used in experiments is just a few monolayers of the tungsten atoms (see also [63], [6], [64]). As a result, for an extremely high hydrogen fluence, Φ_H, the amount of hydrogen trapped in tungsten does not saturate and scales as $\sqrt{\Phi_H}$ [65].

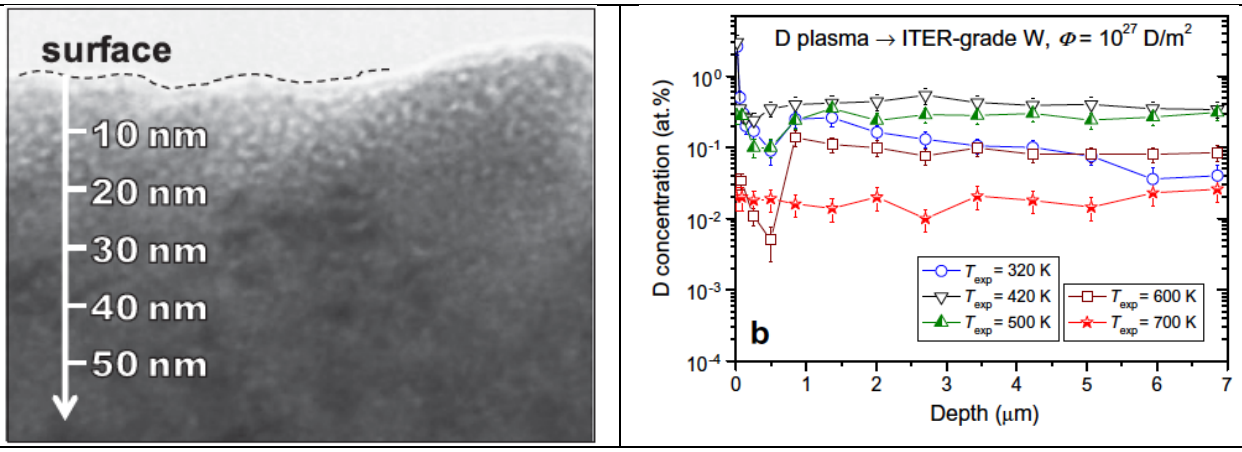

Fig. III.9. On the left: the TEM picture of the layer of He nano-bubbles (Reproduced with permission from [60], © Elsevier 2011); on the right: NRA measurements of H depth profile (Reproduced with permission from [61], © Elsevier 2012).

Even though massive MD simulation of helium transport in tungsten [66] also shows shallow penetration of helium into tungsten, it would be superficial to conclude that this is solely due to the helium self-trapping mechanism discussed above. The reason for such doubts is the fact that the thickness of the helium layer, ℓ_{He}, is virtually independent of the helium flux to the target, j_{He}. However, the variation of the helium flux should inevitably result in the proportional variation of the density of free helium in the implantation layer, $[He]_f^{imp} \propto j_{He}$. Since helium transport obeys the RD equations with quadratic sink terms describing the helium self-trapping reactions, one can find that $\ell_{He} \propto 1/\sqrt{j_{He}}$ [67]. Recalling that in Ref. [62] j_{He} has varied by four orders of magnitude, the helium self-trapping mechanism should result in a two orders of magnitude difference in ℓ_{He}, which contradicts the experimental observations. A possible reconciliation of the experimental data with their theoretical interpretation could be related to the following effects, which are not allowed for in the simple analysis based on the form of the RD equations. First, one can assume that the seeds for helium nano-bubble nucleation are formed by the pre-existing lattice defects. In this case, ℓ_{He} would be inversely proportional to the defect density. The second one takes into account the MD simulation results showing that the growth of the helium nano-bubbles on its own produces lattice defects [68], [15], [58], which could serve as the helium trapping and nano-bubble nucleation sites [51]. As a result, an avalanche effect occurs (growing nano-bubble produces seeds for nucleation of another nano-bubble), which

makes the final evolution of the formation of the helium nano-bubble layer very weakly dependent on the particular initial helium trapping mechanism, which provides the initial seed for the helium bubbles, and, therefore, on the magnitude of j_{He} [51] (although the time needed to form such a layer is inversely proportional to j_{He}, which implies, in agreement with the experimental data, a fixed helium fluence).

Finally, it is conceivable that the formation of a large amount of helium clusters very close to the surface, which is observed in MD simulations at some orientations of the tungsten crystal [69], inhibits deeper penetration of helium.

At the target temperatures below 1000 K, the helium-reach layer does not exhibit visible macroscopic change at helium fluence, Φ_{He}, above Φ_{layer}. It is plausible that this is due to the so-called "bursting" of the nano-bubbles situated just beneath the surface, which is observed in the MD simulations (e.g. see [70]). As a result of such bursting, the very first layer of the nano-bubbles becomes actually open voids, which stop penetration of low-energetic helium deeper into the target and effectively "freeze" the whole nano-bubble layer.

However, the situation becomes very different for the tungsten temperatures in the range between 1000 and 2000 K. Instead of having a "freezed" layer of the nano-bubbles at the fluence $\Phi_{He} > \Phi_{layer}$, nano-tendrils with diameter ~10 nm with some embedded helium nano-bubbles start to grow from the surface (see Fig. III.10) forming the so-called "fuzz" and individual trees of nano-tendrils (e.g. see [73], [74], [5], [72]). According to the experimental data, the thickness of the fuzz is proportional to $\left(\Phi_{He} - \Phi_{layer}\right)^{1/2}$ [62]. We notice that similar growth of nano-tendrils under helium irradiation was observed on many metals including Mo, Ta, Fe, Ni, Ti, etc., which indicates that fuzz formation exhibits very general features of helium interaction with metals (see corresponding references in [24]).

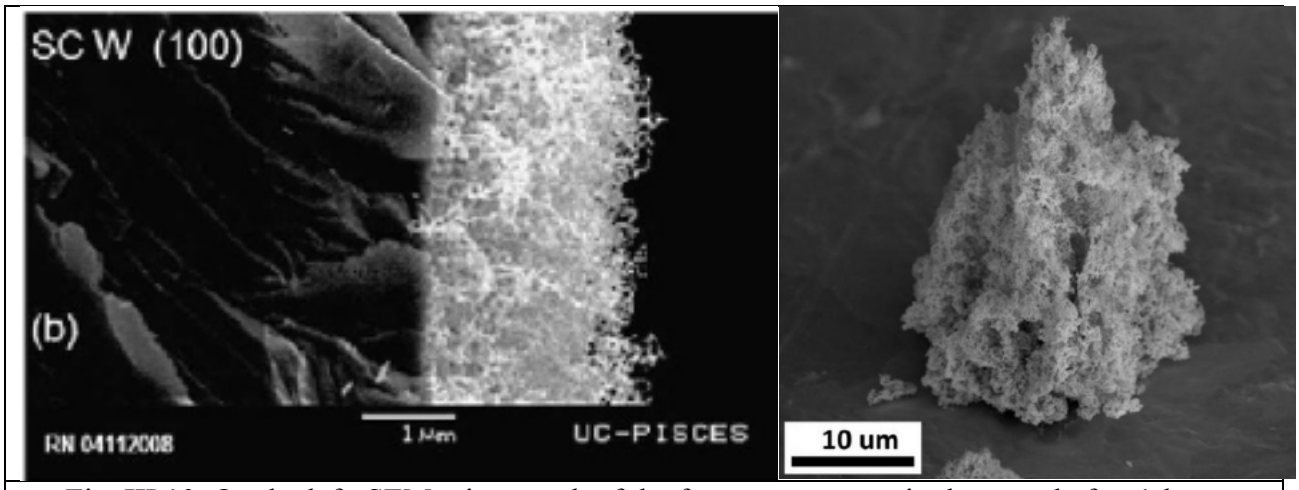

Fig. III.10. On the left: SEM micrograph of the fuzz grown on a single crystal after 1-hour irradiation by 40 eV helium ions (Reproduced with permission from [71], © Elsevier 2010) and on the right: individual tree of nano-tendrils (Reproduced with permission from [72], © Elsevier 2017) grown on a tungsten surface exposed to 50 eV helium ion irradiation.

Although few mechanisms of nano-tendrils growth have been suggested (see related references in [24] for details), neither of them can explain the whole set of the available experimental data. Most probably, the fuzz growth is related to large stresses imposed in the bulk material by continuously growing helium bubbles, which results in plastic deformation of the lattice. Recent experimental observations of a strong material mixture in both tendrils and the bulk [75], [76] seem to support this idea.

Let us now discuss hydrogen transport in tungsten. Even though interstitial hydrogen does not exhibit self-trapping effects, the experimental data show its rather strong accumulation in the tungsten lattice (e.g. see Fig. III.9). Therefore, some other hydrogen trapping mechanism(-s) should exist. One of the possible candidates is hydrogen trapping in the vacancies. The DFT simulations (e.g. see [77], [78], [79], [80] and the references therein) show that a mono-vacancy at room temperature could trap ~ 6 hydrogen atoms with the binding energy ~ 1 eV. Moreover, a combination of the DFT results and thermodynamic consideration suggests that a large amount of hydrogen embedded into a metal lattice (including tungsten) strongly promotes the vacancy formation and buildup of the so-called superabundant vacancies (SAV). Experimental results, although involving the metals with the face-centered cubic lattice such as palladium, nickel, and some others, seem to support the hydrogen-induced formation of SAV (see [81], [82]). The trapping energies ~ 1 eV, similar to those found from the DFT calculations for hydrogen trapping in a mono-vacancy in tungsten, are usually inferred from the TDS data (e.g. see [83], [44], [84], [85]), although in some cases other traps, in particular, with a higher, ~ 2 eV, trapping energy are needed to fit the entire TDS. Traps with E_{tr}~2 eV are usually attributed to hydrogen trapping in voids.

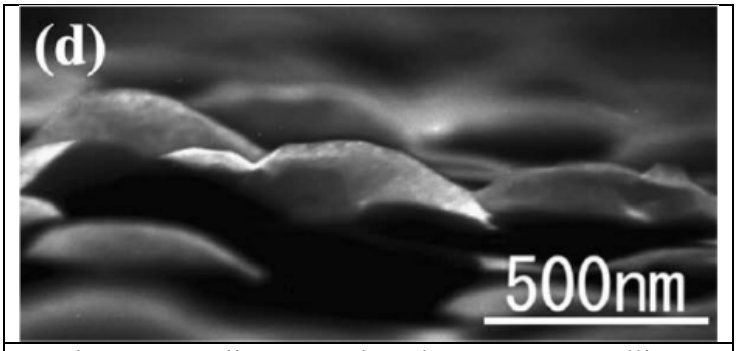

Fig. III.11. Blisters produced on monocrystalline tungsten by 1.5 keV deuterium ion irradiation at the sample temperature of 400 K. Reproduced with permission from [90], © Elsevier 2011.

Other possible trapping sites for hydrogen are related to dislocations. The DTF simulations show that three hydrogen atoms can be bound to the jogs of a screw dislocation (e.g. see [86]) in tungsten with the binding energy ~ 1.4 eV [87], [88] although the further increase of the number of the hydrogen atoms decreases the binding energy significantly. The TEM images demonstrate indeed the presence of screw dislocations decorated by hydrogen clusters [87]. Moreover, they also suggest that the formation of these dislocations, even in a monocrystalline sample, is facilitated by hydrogen [64]. In [89], the MD modeling of hydrogen interactions with both the edge and screw dislocations in tungsten demonstrated a hydrogen-induced modification of the tungsten lattice in the vicinity of the dislocations, formation of dynamic platelet-like hydrogen-reach structures with the hydrogen trapping energy E_{tr}~1 eV. The amount of hydrogen trapped in such platelet structures depends on the tungsten temperature and the hydrogen concentration. In contrast to hydrogen trapping in a vacancy, at low temperatures, hydrogen trapping in platelets related to a dislocation can greatly exceed 100 hydrogen atoms per a dislocation segment. It is conceivable that the temporal evolution of such platelets can account for the growth of the blisters observed experimentally under hydrogen irradiation of tungsten and some other metals at relatively low temperatures (see

Fig. III.11). Formation of similar platelet-like structures could also be triggered by the presence in the sample of the non-hydrostatic tensile and shear stress components. We notice that an impact of a strain applied to the tungsten lattice on the hydrogen solution energy, found from the DFT simulations, was also reported in [54].

Neutron irradiation of tungsten, unavoidable in fusion reactors, results in tungsten lattice damage and the formation of a large amount of additional hydrogen traps. However, experiments with neutron-irradiated samples can only be done just in a few laboratories (e.g. see [91], [92]). Therefore, some energetic ion (such as Si, He, Cu, W, etc.) irradiation is often used as a proxy for the neutron damage [93], [63], [94], [92], [52], [6], [95]. The available experimental data demonstrate that the lattice damage causes a large increase of trapped hydrogen although the comparison of hydrogen retention in the neutron- and ion-damaged tungsten samples shows a significant difference in the corresponding TDS peaks [92]. This could suggest different structures of the lattice damage imposed by neutrons and energetic ions. However, annealing of the damaged samples at high temperature before hydrogen irradiation strongly reduces the impact of the lattice damage on hydrogen retention [94].

In fusion plasma, hydrogen is always accompanied by helium (the fusion ash). Possible synergistic effects of tungsten irradiation by low energy hydrogen with small admixture of helium ions on hydrogen retention were studied both experimentally and theoretically [63], [96], [97], [98], [99], [100], [101], [102], [103]. All these studies show that an admixture of even small (~5%) of helium results in a strong reduction of the amount of retained hydrogen, which could be attributed to the binding of hydrogen to helium nano-bubbles close to the surface, as seem to be indicated by some experimental data and simulations. However, this effect could also be related to possible interconnections of helium nano-bubbles resulting in a back leakage of hydrogen [104].

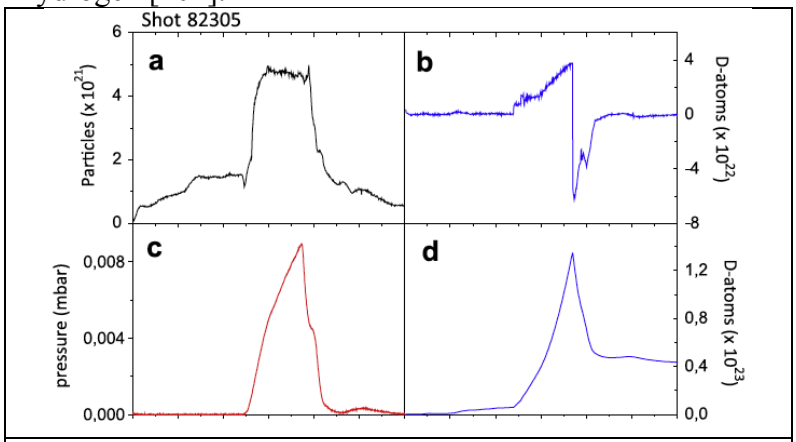

Fig. III.12. Temporal variation of (a) number of plasma particles, (b) dynamic wall retention, (c) neutral pressure in the sub-divertor region, and (d) cumulative wall retention, in a JET discharge. Reproduced with permission from [116], © Elsevier 2013.

Another PFM used in fusion devices is beryllium. Although the beryllium crystal structure, hexagonal close-packed, is very different from the body-centered cubic lattice of tungsten, the DFT simulations show that only up to five hydrogen atoms could be trapped in a beryllium lattice vacancy with the de-trapping energy ~1.7 eV [105], [106]. The trapping energies from 1.25 to 2 eV were also deduced from the analysis of the TDS data (e.g. see [107]). However, unlike tungsten, where the amount of trapped hydrogen is increasing with Φ_H [65], the amount of hydrogen retained in beryllium saturates with Φ_H at a relatively low value [108], [101]. This is probably due to the formation of interconnected hydrogen nano-bubbles creating a porous structure in a rather thin sub-surface layer [109], 110], [108]. However, due to relatively high erosion of beryllium, the beryllium co-deposits (formed from the eroded beryllium atoms transported to and deposited at some particular locations in fusion

devices) are the main sources of retained hydrogen in beryllium-containing tokamaks such as JET [40], [3], [101]. Similarly, for the case of carbon-based tokamaks, the main reservoir of retained hydrogen was in carbon co-deposits (e.g. see [2] and the references therein). According to [40], [111], beryllium co-deposits formed at relatively low temperature have an amorphous structure.

Interestingly, the hydrogen outgassing flux from the PFM at a constant temperature, Γ_{out}, from different tokamaks with both beryllium and carbon co-deposits exhibit (varying by orders of magnitude) similar temporal dependence $\Gamma_{out}(t) \propto t^{-\alpha}$ with $\alpha \approx 0.7$ [112], [113], [114], [3]. Whereas the tokamak data could be related to some peculiarities of wall loading with hydrogen, laboratory experiments with a constant deposition rate also demonstrate the power-law temporal dependence of $\Gamma_{out}(t)$ with similar values of α [115]. We notice that the standard diffusion law would give $\alpha = 0.5$. The physical reason for such an unexpected dependence of $\Gamma_{out}(t)$ is not clear. It is plausible that the amorphous co-deposits have a rather broad band of hydrogen trapping energies so that hydrogen transport can finally be described with fractional diffusion equations resulting in $\alpha \neq 0.5$ [46].

However, during a discharge, both the hydrogen outgassing flux from the PFM and the wall uptake have a much more complex temporal behavior [116], [117]. As an example, from Fig. III.12 one can see, how the dynamic particle (hydrogen) exchange between the plasma and the wall structures during a discharge in the JET tokamak actually works.

Finally, we discuss briefly the usage of lithium as the material for the PFCs (e.g. see [22] and the references therein). Lithium (both solid and liquid) is used for the PFCs in fusion-related experiments (including tokamaks [118], [119], [120], [121], [122]) for more than a decade. One of the clear advantages of lithium is low Z, which makes it rather benign from the point of view of plasma contamination. It is difficult to predict whether lithium will be used in future fusion devices (but see [123]), but these days lithium becomes more and more popular in the fusion community as, at least, a tool for improving tokamak performance and solving some current issues with the PFM. Liquid lithium is a subject of both Bénard-Marangoni convection (caused by temperature-dependent surface tension) and $\vec{j} \times \vec{B}$ force, where the electric current $\vec{j}$ could be driven by both the plasma and the thermoelectric effects. The latter ones could be used to induce the lithium flow [124] allowing to avoid lithium overheating by the plasma that results in the excessive lithium influx into the plasma. However, large uncontrolled plasma currents during ELMs can splash the freely flowing lithium into the plasma, which can terminate the discharge. An alternative way of introducing lithium for the PFM is to use some porous structure so that lithium would wet up the front surface of this structure but would still be confined by the pores [118], [119]. Virtually all the available experimental data from current tokamaks using, in some way, lithium report a significant reduction of plasma contamination with impurity and improvement of core plasma confinement. However, lithium is a strong absorber of the hydrogen isotopes. Therefore, to maintain the tritium budget, the application of lithium in future reactors would require virtually complete tritium recovery from lithium. However, on the other hand, strong absorption of hydrogen can, potentially, open the way to a new, very favorable "zero-recycling" operational regime of a tokamak [125]. Recent experimental data seem to show that such a regime could indeed exist [121].

Conclusions for Ch. III

In conclusion to this chapter, it would be fair to say that the situation with the plasma-material interactions and material-related effects is far from being satisfactory and much more should be done in this area. Whereas we understand rather well the basic features of particle reflection from the material targets and physical sputtering, it is still difficult to make quantitative predictions of both reflection and sputtering for the case where the constituency of the first atomic layers of the wall material is evolving in time due to the plasma-material interactions. The situation becomes even worse if we need to make an assessment of helium and hydrogen transport in the material lattice. It seems that we understand the basics of the helium trapping mechanism at relatively low target temperatures, but we are yet unable to provide reliable models of the growth of fuzzy structures when the temperature goes up. For hydrogen transport and retention in tungsten, few primary mechanisms of hydrogen trapping were identified (e.g. SAV, dislocations). But still, no definite conclusion has been reached among the scientific community. In addition, there are some indications of a possible nonlinear, hydrogen-induced generation of the traps, but there is no quantitative predictive theoretical model that could be challenged by the experimental data yet. Interestingly, the experimental data on hydrogen retention in tungsten, for the conditions excluding such unwanted and complex effects as blistering, suggest that for extremely high hydrogen fluence, Φ_H, the amount of trapped hydrogen is simply proportional to $\sqrt{\Phi_H}$ [65].

References for Chapter III

[1] D. Stork and S. J. Zinkle, "Introduction to the special issue on the technical status of materials for a fusion reactor", Nucl. Fusion **57** (2017) 092001.

[2] J. Roth, E. Tsitrone, A. Loarte, Th. Loarer, G. Counsell, R. Neu, V. Philipps, S. Brezinsek, M. Lehnen, P. Coad, Ch. Grisolia, K. Schmid, K. Krieger, A. Kallenbach, B. Lipschultz, R. Doerner, R. Causey, V. Alimov, W. Shu, O. Ogorodnikova, A. Kirschner, G. Federici, A. Kukushkin, EFDA PWI Task Force, ITER PWI Team, Fusion for Energy, ITPA SOL/DIV, "Recent analysis of key Plasma Wall Interactions issues for ITER", J. Nucl. Mater. **390-391** (2009) 1-9.

[3] S. Brezinsek, T. Loarer, V. Philipps, H. G. Esser, S. Grűnhagen, R. Smith, R. Felton, J. Banks, P. Belo, A. Boboc, J. Bucalossi, M. Clever, J.W. Coenen, I. Coffey, S. Devaux, D. Douai, M. Freisinger, D. Frigione, M. Groth, A. Huber, J. Hobirk, S. Jachmich, S. Knipe, K. Krieger, U. Kruezi, S. Marsen, G.F. Matthews, A.G. Meigs, F. Nave, I. Nunes, R. Neu, J. Roth, M. F. Stamp, S. Vartanian, U. Samm and JET EFDA contributors, "Fuel retention studies with the ITER-Like Wall in JET", Nucl. Fusion **53** (2013) 083023.

[4] P. Roubin, B. Pégourié, R. Smirnov, C. Martin, M. Richou, Y. Marandet, C. Pardanaud, C. Brosset, J. Gunn, "Analysis of carbon deposited layer growth processes in Tore Supra", J. Nucl. Mater. **390-391** (2009) 49-52.

[5] S. Kajita, W. Sakaguchi, N. Ohno, N. Yoshida and T. Saeki, "Formation process of tungsten nanostructure by the exposure to helium plasma under fusion relevant plasma conditions", Nucl. Fusion **49** (2009) 095005.

[6] T. Tanabe, "Review of hydrogen retention in tungsten", Phys. Scr. **T159** (2014) 014044.

[7] P. Hohenberg and W. Kohn, "Inhomogeneous electron gas", Phys. Rev. **136** (1964) B864-B871.

[8] http://www.quantum-espresso.org/

[9] G. Kresse and J. Hafner, "*Ab initio* molecular dynamics for liquid metals", Phys. Rev. B **47** (1993) 558-561.

[10] http://lammps.sandia.gov./

[11] W. Mller, W. Eckstein, "Tridyn-binary collision simulation of atomic collisions and dynamic composition changes in solids", Comp. Phys. Comm. **51** (1988) 355-368.

[12] G. R. Longhurst, "TMAP7 Manual," INEEL/EXT-04-02352, Idaho National Engineering and Environmental Laboratory, Bechtel BWXT Idaho, LLC (2004).

[13] Brad J. Merrill, Masashi Shimada, Paul W. Humrickhouse, "Simulating Tritium Retention in Tungsten with a Multiple Trap Model in the TMAP Code", J. Plasma Fusion Res. **10** (2013) 71-75.

[14] R. D. Smirnov, J. Guterl, and S. I. Krasheninnikov, "Modeling of Multispecies Dynamics in Fusion-Related Materials with FACE", Fusion Science Tech. **71** (2017) 75-83.

[15] R. D. Smirnov, S. I. Krasheninnikov, J. Guterl, "Atomistic modeling of growth and coalescence of helium nano-bubbles in tungsten", J. Nucl. Mater. **463** (2015) 359-362.

[16] J. Guterl, R. D. Smirnov, S. I. Krasheninnikov, B. Uberuaga, A. F. Voter, D. Perez, "Modeling of hydrogen desorption from tungsten surface", J. Nucl. Mater. **463** (2015) 263-267.

[17] G. Federici, C. H. Skinner, J. N. Brooks, J. P. Coad, C. Grisolia, A. A. Haasz, A. Hassanein, V. Philipps, C. S. Pitcher, J. Roth, W. R. Wampler, D. G. Whyte, "Plasma-material Interactions in Current Tokamaks and their Implications for Next-step Fusion Reactors", Nucl. Fusion **41** (2001) 1967-2137.

[18] “Nuclear Fusion Research: Understanding Plasma-Surface Interactions” R. E. Clark, D. H. Reiter (Eds) Springer Series in Chemical Physics, **78**, Springer-Verlag, Berlin Heidelberg 2005.
[19] “Sputtering by Particle Bombardment”, R. Behrisch, W. Eckstein (Eds.): Topics Appl. Phys. **110** (2007), Springer-Verlag, Berlin Heidelberg 2007.
[20] J. Roth, E. Tsitrone, A. Loarte, “Plasma–wall interaction: Important ion induced surface processes and strategy of the EU Task Force”, Nucl. Instr. Methods in Phys. Res. B **258** (2007) 253-263.
[21] B. D. Wirth, K. D. Hammond, S. I. Krasheninnikov, D. Maroudas, “Challenges and opportunities of modeling plasma–surface interactions in tungsten using high-performance computing”, J. Nucl. Mater. **463** (2015) 30-38.
[22] R. E. Nygren, F. L. Tabares, “Liquid surfaces for fusion plasma facing components—A critical review. Part I: Physics and PSI”, Nucl. Mater. Energy **9** (2016) 6-21.
[23] G. Federici, W. Biel, M.R. Gilbert, R. Kemp, N. Taylor and R. Wenninger, “European DEMO design strategy and consequences for materials”, Nucl. Fusion **57** (2017) 092002.
[24] K. Hammond, “Helium, hydrogen, and fuzz in plasma-facing materials”, Mater. Res. Express **4** (2017) 104002.
[25] Y. Ueda, K. Schmid, M. Balden, J.W. Coenen, Th. Loewenhoff, A. Ito, A. Hasegawa, C. Hardie, M. Porton and M. Gilbert, “Baseline high heat flux and plasma facing materials for fusion”, Nucl. Fusion **57** (2017) 092006
[26] E. W. Thomas, R. K. Janev and J. Smith, “Scaling of particle reflection coefficients”, Nucl. Instr. Meth. Phys. Res. B **69** (1992) 427-436.
[27] W. D. Wilson and R. A. Johnson, in “Interatomic Potentials and Simulation of Lattice Defects”, edited by P. C. Gehlen, J. R. Heeler, and R. I. Jaffee (Plenum, New York, 1972).
[28] R. Frauenfelder, “Solution and Diffusion of Hydrogen in Tungsten”, J. Vac. Sci. Technol. **6** (1969) 388-397.
[29] R. S. Nelson, “An investigation of thermal spikes by studying the high energy sputtering of metals at elevated temperatures”, Phil. Magazine **11**(110) (1965) 291-302.
[30] E. P. Vaulin, N. E. Georgieva, T. P. Martynenko, L.V. Feoktistov, “Erosion of hot refractory metals caused by low-energy ions”, Sov. J. Plasma Phys. **7** (1981) 239-242.
[31] V. Philipps, K. Flaskamp, E. Vietzke, “Enhancement of the sputtering yield of pyrolytic graphite at elevated temperatures”, J. Nucl. Mater. **111-112** (1982) 781-784.
[32] R. P. Doerner, S. I. Krasheninnikov, K. Schmid, “Particle-induced erosion of materials at elevated temperature”, J. Appl. Phys. **95** (2004) 4471-4475.
[33] R. P. Doerner, M. J. Baldwin, S. Krasheninnikov, D. G. Whyte, “Behavior of high temperature liquid surfaces in contact with plasma”, J. Nucl. Mater. **313-316** (2003) 383-387.
[34] J. P. Allain, J. N. Brooks, D. A. Alman, L.E. Gonzalez, “Model development and analysis of temperature-dependent lithium sputtering and sputtered Li^+ transport for tokamak plasma-facing applications”, J. Nucl. Mater. **337-339** (2005) 94-98.
[35] R. W. Conn, R. P. Doerner, F. C. Sze, S. Luckhardt, A. Liebscher, R. Seraydarian and D. G. Whyte, “Deuterium plasma interactions with liquid gallium”, Nucl. Fusion **42** (2002) 1060-1066.
[36] A. von Hippel, “Zur Theorie der Kathodenzerstäubung”, Ann. d. Physik. **81** (1926) 1043-1075.
[37] J. Roth and W. Möller, “Mechanism of enhanced sputtering of carbon at temperatures above 1200°C”, Nucl. Instrum. Methods Phys. Res. B **7-8** (1985) 788-792.

[38] M. W. Thompson, "III. The energy spectrum of ejected atoms during the high energy sputtering of gold", Philos. Mag. **18** (1968) 377-414.
[39] M. W. Thompson, "The velocity distribution of sputtered atoms", Nucl. Instrum. Methods Phys. Res. B **18** (1987) 411-429.
[40] R. P. Doerner, M. J. Baldwin, D. Buchenauer, G. De Temmerman, D. Nishijima, "The role of beryllium deuteride in plasma-beryllium interactions", J. Nucl. Mater. **390-391** (2009) 681-684.
[41] M. Poon, A. A. Haasz, J. W. Davis, "Modelling deuterium release during thermal desorption of D^+-irradiated tungsten", J. Nucl. Mater. **374** (2008) 390-402.
[42] J. Roth and K. Schmid, "Hydrogen in tungsten as plasma-facing material", Phys. Scripta **T145** (2011) 014031.
[43] Yu. M. Gasparyan, O. V. Ogorodnikova, V. S. Efimov, A. Mednikov, E. D. Marenkov, A. A. Pisarev, S. Markelj, I. Čadež, "Thermal desorption from self-damaged tungsten exposed to deuterium atoms", J. Nucl. Mater. **463** (2015) 1013-1016
[44] O. V. Ogorodnikova, "Fundamental aspects of deuterium retention in tungsten at high flux plasma exposure", J. Appl. Physics **118** (2015) 074902.
[45] A. Jakobs, K. W. Kehr, "Theory and simulation of multiple-trapping transport through a finite slab", Phys. Rev. B **48** (1993) 8780-8789.
[46] S. I. Krasheninnikov, E. D. Marenkov, "On hydrogen transport in the first wall material of fusion devices in the presence of a broadband distribution of traps over the trapping energy", Phys. Lett. A **378** (2014) 1526-1530.
[47] K. Schmid, U. von Toussaint, and T. Schwarz-Selinger, "Transport of hydrogen in metals with occupancy dependent trap energies", J. Appl. Phys. **116** (2014) 134901.
[48] L. Hu, K. D. Hammond, B. D. Wirth, D. Maroudas, "Dynamics of small mobile helium clusters near tungsten surfaces", Surface Science **626** (2014) L21-L25.
[49] Q. Hu, S. Sharafat, N. M. Ghoniem, "Modeling space-time dependent helium bubble evolution in tungsten armor under IFE conditions", Fus. Sci. Technol. **52** (2007) 574-578.
[50] D. Xu and B. D. Wirth, "Modeling spatially dependent kinetics of helium desorption in BCC iron following He ion implantation", J. Nucl. Mater. **403** (2010) 184-190.
[51] S. I. Krasheninnikov and R. D. Smirnov, "He cluster dynamics in fusion related plasma facing materials", Nucl. Fusion **55** (2015) 073005.
[52] M. H. J. 't Hoen, M. Mayer, A.W. Kleyn, H. Schut and P. A. Z. van Emmichoven, "Strongly Reduced Penetration of Atomic Deuterium in Radiation-Damaged Tungsten", Phys. Rev. Lett. **111** (2013) 225001.
[53] D. Perez, T. Vogel, and B. P. Uberuaga, "Diffusion and transformation kinetics of small helium clusters in bulk tungsten", Phys. Rev. B **90** (2014) 014102.
[54] W. G.-H. Lu, H.-B. Zhou, and C. S. Becquart, "A review of modelling and simulation of hydrogen behaviour in tungsten at different scales", Nucl. Fusion **54** (2014) 086001.
[55] L. M. Caspers, R. H. J. Fastenau, A. van Veen, and W. F. W. M. van Heugten, "Mutation of vacancies to divacancies by helium trapping in molybdenum effect on the onset of percolation", Phys. Status Solidi A **46** (1978) 541-546.
[56] M. I. Baskes, R. H. J. Fastenau, P. Penning, L. M. Caspers, A. van Veen, "On the low-temperature nucleation and growth of bubbles by helium bombardment of metals", J. Nucl. Mater. **102** (1981) 235-245.
[57] K. O. E. Henriksson, K. Nordlund, J. Keinonen, "Molecular dynamics simulations of helium cluster formation in tungsten", Nucl. Instr. Meth. Phys. Res. B **244** (2006) 377-391.

[58] D. Perez, L. Sandoval, B. P. Uberuaga, and A. F. Voter, "The thermodynamic and kinetic interactions of He interstitial clusters with bubbles in W", J. Appl. Phys. **119** (2016) 203301.
[59] Y. Z. Jia, W. Liu, B. Xu, S. L. Qu, L. Q. Shi and T. W. Morgan, "Subsurface deuterium bubble formation in W due to low-energy high flux deuterium plasma exposure", Nucl. Fusion **57** (2017) 034003.
[60] M. Miyamoto, D. Nishijima, M. J. Baldwin, R. P. Doerner, Y. Ueda, K. Yasunaga, N. Yoshida, K. Ono, "Microscopic damage of tungsten exposed to deuterium-hydrogen mixture plasma in PISCES and its impacts on retention property", J. Nucl. Mater. **415** (2011) S657-S660.
[61] V. Kh. Alimov, B. Tyburska-Püschel, S. Lindig, Y. Hatano, M. Balden, J. Roth, K. Isobe, M. Matsuyama, T. Yamanishi, "Temperature dependence of surface morphology and deuterium retention in polycrystalline ITER-grade tungsten exposed to low-energy, high-flux D plasma", J. Nucl. Mater. **420** (2012) 519-524.
[62] T. J. Petty, M. J. Baldwin, M. I. Hasan, R. P. Doerner and J. W. Bradley, "Tungsten 'fuzz' growth re-examined: the dependence on ion fluence in non-erosive and erosive helium plasma", Nucl. Fusion **55** (2015) 093033.
[63] W. R. Wampler and R. P. Doerner, "The influence of displacement damage on deuterium retention in tungsten exposed to plasma", Nucl. Fusion **49** (2009) 115023.
[64] D. Terentyev, A. Dubinko, A. Bakaeva, G. De Temmerman, "Strong sub-surface plastic deformation induced by high flux plasma in tungsten", Fus. Eng. Design **124** (2017) 405-409.
[65] R. P. Doerner , M.J. Baldwin, T.C. Lynch, J.H. Yu, "Retention in tungsten resulting from extremely high fluence plasma exposure", Nucl. Mater. Energ. **9** (2016) 89-92.
[66] K. D. Hammond, S. Blondel, L. Hu, D. Maroudas, B. D. Wirth, "Large-scale atomistic simulations of low-energy helium implantation into tungsten single crystals", Acta Mater. **144** (2018) 561-578.
[67] S. I. Krasheninnikov, T. Farley and B. D. Wirth, "On helium cluster dynamics in tungsten plasma facing components of fusion devices", Nucl. Fusion **54** (2014) 073019.
[68] F. Sefta, K. D. Hammond, N. Juslin and B. D.Wirth, "Tungsten surface evolution by helium bubble nucleation, growth and rupture", Nucl. Fusion **53** (2013) 073015.
[69] K. D. Hammond and B. D. Wirth, "Erratum: "Crystal orientation effects on helium ion depth distributions and adatom formation processes in plasma-facing tungsten" [J. Appl. Phys. 116, 143301 (2014)]", J. Appl. Phys. **116** (2014) 143301.
[70] F. Sefta, N. Juslin, and B. D.Wirth, "Helium bubble bursting in tungsten", J. Appl. Phys. **114** (2013) 243518.
[71] M. J. Baldwin and R. P. Doerner, "Formation of helium induced nanostructure 'fuzz' on various tungsten grades", J. Nucl. Mater. **404** (2010) 165-173.
[72] K. B. Woller, D. G. Whyte, G. M. Wright, "Isolated nano-tendril bundles on tungsten surfaces exposed to radiofrequency helium plasma", Nucl. Mater. Energy **12** (2017) 1282-1287.
[73] S. Takamura, N. Ohno, D. Nishijima and S. Kajita, "Formation of Nanostructured Tungsten with Arborescent Shape due to Helium Plasma Irradiation", Plasma Fusion Res. **1** (2006) 051.
[74] M. J. Baldwin and R. P. Doerner, "Helium induced nanoscopic morphology on tungsten under fusion relevant plasma conditions", Nucl. Fusion **48** (2008) 035001.
[75] P. Fiflis, N. Connolly and D. N. Ruzic, "Experimental mechanistic investigation of the

nanostructuring of tungsten with low energy helium plasmas", J. Nucl. Mater. **482** (2016) 201.
[76] R.P. Doerner, D. Nishijima, S. I. Krasheninnikov, T. Schwarz-Selinger and M. Zach, "Motion of W and He atoms during formation of W fuzz", Nucl. Fusion **58** (2018) 066005.
[77] K. Heinola, T. Ahlgren, K. Nordlund, and J. Keinonen, "Hydrogen interaction with point defects in tungsten", Phys. Rev. B **82** (2010) 094102.
[78] Y.-L. Liu, H.-B. Zhou, Y. Zhang, "Investigating behaviors of H in a W single crystal by first-principles: From solubility to interaction with vacancy", J. Alloys Compd. **509** (2011) 8277-8282.
[79] K. Ohsawa, K. Eguchi, H. Watanabe, M. Yamaguchi, M. Yagi, "Configuration and binding energy of multiple hydrogen atoms trapped in monovacancy in bcc transition metals", Phys. Rev. B **85** (2012) 094102.
[80] N. Fernandez, Y. Ferro, and D. Kato, "Hydrogen diffusion and vacancies formation in tungsten: Density Functional Theory calculations and statistical models", Acta Materialia **94** (2015) 307-318.
[81] Y. Fukai and N. Okuma, "Formation of Superabundant Vacancies in Pd Hydride under High Hydrogen Pressures", Phys. Rev. Lett. **73** (1994) 1640-1643.
[82] Y. Fukai, "Formation of superabundant vacancies in M–H alloys and some of its consequences: a review", J. Alloys Compd. **356–357** (2003) 263-269.
[83] D. F. Johnson, E. A. Carter, "Hydrogen in tungsten: Absorption, diffusion, vacancy trapping, and decohesion", J. Mater. Res. **25** (2010) 315-327.
[84] J. Guterl, R. D. Smirnov, S. I. Krasheninnikov, M. Zibrov and A. A. Pisarev, "Theoretical analysis of deuterium retention in tungsten plasma-facing components induced by various traps via thermal desorption spectroscopy", Nucl. Fusion **55** (2015) 093017.
[85] E. A. Hodille, Y. Ferro, N. Fernandez, C. S. Becquart, T. Angot, J. M. Layet, R. Bisson and C. Grisolia, "Study of hydrogen isotopes behavior in tungsten by a multi trapping macroscopic rate equation model", Phys. Scripta **T167** (2016) 014011.
[86] W. Cai and W. D. Nix, "Imperfections in crystalline solids", Cambridge, United Kingdom: Cambridge University Press, 2016.
[87] D. Terentyev, V. Dubinko, A. Bakaev, Y. Zayachuk, W. Van Renterghem and P. Grigorev, "Dislocations mediate hydrogen retention in tungsten", Nucl. Fusion **54** (2014) 042004.
[88] V. I. Dubinko, P. Grigorev, A. Bakaev, D. Terentyev, G. van Oost, F. Gao, D. Van Neck and E. E. Zhurkin, "Dislocation mechanism of deuterium retention in tungsten under plasma implantation", J. Phys.: Condens. Matter **26** (2014) 395001.
[89] R. D. Smirnov and S. I. Krasheninnikov, "Stress-induced hydrogen self-trapping in tungsten", Nucl. Fusion **58** (2018) 126016.
[90] N. Enomoto, S. Muto, and T. Tanabe "Grazing-incidence electron microscopy of surface blisters in single- and polycrystalline tungsten formed by H^+, D^+ and He^+ irradiation", J. Nucl. Mater **385** (2009) 606-614.
[91] M. Shimada, G. Cao, Y. Hatano, T. Oda, Y. Oya, M. Hara and P. Calderoni, "The deuterium depth profile in neutron-irradiated tungsten exposed to plasma", Phys. Scripta **T145** (2011) 014051.
[92] M. Shimada, Y. Hatano, Y. Oya, T. Oda, M. Hara, G. Cao, M. Kobayashi, M. Sokolov, H. Watanabe, B. Tyburska-Püschel, Y. Ueda, P. Calderoni, K. Okuno, "Overview of theUS–Japan collaborative investigation on hydrogen isotope retention in neutron-irradiated and ion-damaged tungsten.", Fus. Eng. Design **87** (2012) 1166.

[93] I. I. Arkhipov, S. L. Kanashenko, V. M. Sharapov, R. Kh. Zalavutdinov, A. E. Gorodetsky, "Deuterium trapping in ion-damaged tungsten single crystal", J. Nucl. Mater. **363–365** (2007) 1168-1172.
[94] B. Tyburska, V. Kh. Alimov, O. V. Ogorodnikova, K. Schmid, K. Ertl, "Deuterium retention in self-damaged tungsten", J. Nucl. Mater. **395** (2009) 150-155.
[95] M. J. Simmonds, Y. Q. Wang, J. L. Barton, M. J. Baldwin, J. H. Yu, R. P. Doerner, G. R. Tynan, "Reduced deuterium retention in simultaneously damaged and annealed tungsten", J. Nucl. Mater. **494** (2017) 67-71.
[96] M. Miyamoto, D. Nishijima, Y. Ueda, R. P. Doerner, H. Kurishita, M. J. Baldwin, S. Morito, K. Ono and J. Hanna, "Observations of suppressed retention and blistering for tungsten exposed to deuterium–helium mixture plasmas", Nucl. Fusion **49** (2009) 065035.
[97] V. Kh. Alimov, W. M. Shu, J. Roth, K. Sugiyama, S. Lindig, M. Balden, K. Isobe and T. Yamanishi, "Surface morphology and deuterium retention in tungsten exposed to low-energy, high flux pure and helium-seeded deuterium plasmas", Phys. Scripta **T138** (2009) 014048.
[98] O. V. Ogorodnikova, T. Schwarz-Selinger, K. Sugiyama and V. Kh. Alimov, "Deuterium retention in tungsten exposed to low-energy pure and helium-seeded deuterium plasmas", J. Appl. Phys. **109** (2011) 013309.
[99] M. J. Baldwin, R. P. Doerner, W. R.Wampler, D. Nishijima, T. Lynch and M. Miyamoto, "Effect of He on D retention in W exposed to low-energy, high-fluence (D, He, Ar) mixture plasmas", Nucl. Fusion **51** (2011) 103021.
[100] N. Juslin, B.D. Wirth, "Molecular dynamics simulation of the effect of sub-surface helium bubbles on hydrogen retention in tungsten", J. Nucl. Mater. **438** (2013) S1221-S1223.
[101] G. Federici, V. Barabash, R. Doerner, P. Lorenzetto, G. Matthews, A.R. Raffray, Reference Module in Materials Science and Materials Engineering, from Comprehensive Nuclear Materials, *2016*, Current as of 22 July 2016.
[102] S. Markelj, T. Schwarz-Selinger and A. Založnik, "Hydrogen isotope accumulation in the helium implantation zone in tungsten", Nucl. Fusion **57** (2017) 064002.
[103] Z. J. Bergstrom, M. A. Cusentino & B. D. Wirth, "A Molecular Dynamics Study of Subsurface Hydrogen-Helium Bubbles in Tungsten", Fus. Sci. Techn. **71** (2017) 122-135.
[104] M. J. Baldwin and R. P. Doerner, "Hydrogen isotope transport across tungsten surfaces exposed to a fusion relevant He ion fluence", Nucl. Fusion **57** (2017) 076031.
[105] M. G. Ganchenkova, V. A. Borodin, and R. M. Nieminen, "Hydrogen in beryllium: Solubility, transport, and trapping", Phys. Rev. B **79** (2009) 134101.
[106] A. Allouche, M. Oberkofler, M. Reinelt, and Ch. Linsmeier, "Quantum Modeling of Hydrogen Retention in Beryllium Bulk and Vacancies", J. Chem. Phys. **114** (2010) 3588-3598.
[107] M. Reinelt, A. Allouche, M. Oberkofler and Ch. Linsmeier, "Retention mechanisms and binding states of deuterium implanted into beryllium", New J. Phys. **11** (2009) 043023.
[108] R. A. Anderl, R. A. Causey, J. W. Davis, R. P. Doerner, G. Federici, A. A. Haasz, G. R. Longhurst, W. R. Wampler, K. L. Wilson, "Hydrogen isotope retention in beryllium for tokamak plasma-facing applications", J. Nucl. Mater. **273** (1999) 1-26.
[109] V. N. Chernikov, V. Kh. Alimov, A. V. Markin, A. P. Zakharov, "Gas swelling and related phenomena in beryllium implanted deuterium ions", J. Nucl. Mater. **228** (1996) 47-60.
110] V. Kh. Alimov, V. N. Chernikov, A. P. Zakharov, "Depth distribution of deuterium atoms and molecules in beryllium implanted with D ions", J. Nucl. Mater. **241-243** (1997) 1047-

1051.
[111] G. De Temmerman, M. J. Baldwin, R. P. Doerner, D. Nishijima, R. Seraydarian, K. Schmid, "Insight into the co-deposition of deuterium with beryllium: Influence of the deposition conditions on the deuterium retention and release", J. Nucl. Mater. **390-391** (2009) 564-567.
[112] V. Philipps and J. Ehrenberg, "Analysis of outgassing after Joint European Torus discharges under beryllium first wall conditions", J. Vac. Sci. Technol. A **11** (1993) 437-445.
[113] V. Philipps, M. Freisinger, A. Huber, T. Loarer, JET EFDA contributors, "Effect of disruptions on fuel release from JET walls", J. Nucl. Mater. **390-391** (2009) 478-481.
[114] B. Pégourié, S. Panayotis, P. Languille, C. Martin, T. Dittmar, E. Gauthier, J.-C. Hatchressian, J.-Y. Pascal, P. Roubin, R. Ruffe, E. Tsitrone, S. Vartanian, H. Wang, A. Beauté, J. Bouvet, C. Brosset, J. Bucalossi, M. Cabié, E. Caprin, X. Courtois, R. Dachicourt, E. Delchambre, C. Dominici, D. Douai, A. Ekedahl, J.P. Gunn, A. Hakola, W. Jacob, H. Khodja, J. Likonen, F. Linez, A. Litnovsky, Y. Marandet, S. Markelj, A. Martinez, M. Mayer, O. Meyer, P. Monier-Garbet, P. Moreau, V. Negrier, P. Oddon, C. Pardanaud, B. Pasqueti, P. Pelicon, P. Petersson, V. Philipps, G. Possnert, D. Reiter, J. Roth, I. Roure, M. Rubel, F. Saint-Laurent, F. Samaille, P. Vavpetič, "Deuterium inventory in Tore Supra: Coupled carbon–deuterium balance", J. Nucl. Mater. **438** (2013) S120-S125.
[115] S. Möller, D. Matveev, Y. Martynova, B. Unterberg, M. Rasinski, T. Wegener, A. Kreter and Ch. Linsmeier, "Dynamic outgassing of deuterium, helium and nitrogen from plasma-facing materials under DEMO relevant conditions", Nucl. Fusion **57** (2017) 016020.
[116] V. Philipps, T. Loarer, H. G. Esser, S. Vartanian, U. Kruezi, S. Brezinsek, G. Matthews, JET EFDA contributors, "Dynamic fuel retention and release under ITER like wall conditions in JET", J. Nucl. Mater. **438** (2013) S1067-S1071.
[117] S. Brezinsek, T. Loarer, V. Philipps, H.G. Esser, S. Grünhagen, R. Smith, R. Felton, J. Banks, P. Belo, A. Boboc, J. Bucalossi, M. Clever, J.W. Coenen, I. Coffey, S. Devaux, D. Douai, M. Freisinger, D. Frigione, M. Groth, A. Huber, J. Hobirk, S. Jachmich, S. Knipe, K. Krieger, U. Kruezi, S. Marsen, G.F. Matthews, A.G. Meigs, F. Nave, I. Nunes, R. Neu, J. Roth, M.F. Stamp, S. Vartanian, U. Samm and JET EFDA contributors, "Fuel retention studies with the ITER-Like Wall in JET" Nucl. Fusion **53** (2013) 083023.
[118] S. V. Mirnov, E. A. Azizov, V. E. Evtikhin, V. B. Lazarev, I. E. Lyublinski, A. V. Vertkov and D. Y. Prokhorov, "Experiments with lithium limiter on T-11M tokamak and applications of the lithium capillary-pore system in future fusion reactor devices", Plasma Phys. Contr. Fusion **48** (2006) 821-837.
[119] G. Mazzitelli, M. L. Apicella, D. Frigione, G. Maddaluno, M. Marinucci, C. Mazzotta, V. Pericoli Ridolfini, M. Romanelli, G. Szepesi, O. Tudisco and FTU Team, "FTU results with a liquid lithium limiter", Nucl. Fusion **51** (2011) 073006.
[120] T. W. Morgan, P. Rindt, G. G. van Eden, V. Kvon, M. A. Jaworski, N. J. L. Cardozo, "Liquid metals as a divertor plasma-facing material explored using the Pilot-PSI and Magnum-PSI linear devices", Plasma Phys. Contr. Fus., **60** (2018) 014025,
[121] D. P. Boyle, R. Majeski, J. C. Schmitt, C. Hansen, R. Kaita, S. Kubota, M. Lucia, and T. D. Rognlien, "Observation of Flat Electron Temperature Profiles in the Lithium Tokamak Experiment", Phys. Rev. Lett. **119** (2017) 015001.
[122] H. W. Kugel, D. Mansfield, R. Maingi, M. G. Bel, R. E. Bell, J. P. Allain, D. Gates, S. Gerhardt, R. Kaita, J. Kallman, S. Kaye, B. LeBlanc, R. Majeski, J. Menard, D. Mueller, M. Ono, S. Paul, R. Raman, A.L. Roquemore, P. W. Ross, S. Sabbagh, H. Schneider, C. H.

Skinner, V. Soukhanovskii , T. Stevenson, J. Timberlake, W.R. Wampler, J. Wilgren, L. Zakharov and the NSTX Team, “Evaporated Lithium Surface Coatings in NSTX”, J. Nucl. Mater. **390-391** (2009) 1000-1009.

[123] R. J. Goldston, R. Myers, J. A. Schwartz, “The lithium vapor box divertor”, Phys. Scr. **T167** (2016) 014017.

[124] D. N. Ruzic, W. Xu, D. Andruczyk and M. A. Jaworski, “Lithium-metal trenches (LiMIT) for heat removal in fusion devices”, Nucl. Fusion **51** (2011) 102002.

[125] S. I. Krasheninnikov, L. E. Zakharov, and G. V. Pereverzev, “On lithium walls and the performance of magnetic fusion devices”, Phys. Plasmas **10** (2003) 1678-1682.